Spin-lattice interaction for ions in low-symmetry sites: The case of Mn^{2+}:$CaCO_3$

Gaston E. Barberis and George Balster Martins
Instituto de Física "Gleb Wataghin," Universidade Estadual de Campinas, 13081, Campinas, São Paulo, Brazil

Rafael Calvo
Instituto de Desarrollo Tecnológico para la Industria Química (Conicet) and Facultad de Bioquímica y Ciencias Biológicas (UNL)-Güemes 3450, 3000 Santa Fe, Argentina

(Received 12 July 1993)

The spin-lattice interaction for Mn^{2+} ions as substitutional impurities in $CaCO_3$ has been studied by electron-paramagnetic-resonance (EPR) experiments in crystals under externally applied uniaxial stresses. The shifts of the EPR lines of Mn^{2+} were measured as a function of the stress applied along the three different directions that accept uniaxial forces in this crystal. The values of six second-order spin-lattice coefficients for the Mn^{2+} site were obtained from the data. We also obtained two conditions relating linear combinations of the other four second-order coefficients. Contributions to the spin-lattice interaction of terms of fourth order in the effective spin have been detected. Our results are used to discuss the effect on the EPR spectrum of the different distortions of the carbonate ions surrounding the Mn^{2+}.

I. INTRODUCTION

Homogeneous static stresses applied to a single crystal may be represented by a tensor X and cause strains in the crystal; these strains are canonically represented by the tensor ϵ. Both tensors are related by the stiffness coefficient, which is a fourth-order tensor. The relationship is expressed as[1]:

$$\varepsilon_{ij}=\sum_{\substack{i,j,\\k,l}} S_{ijkl}X_{kl} \ . \tag{1}$$

Stresses (strains) modify the crystal field in the site of magnetic atoms contained in the crystal. When the applied stresses are small, we can write the spin-lattice interaction as[2-4]

$$\mathcal{H}_{\rm SL}=\sum_{\substack{n,i,\alpha\\ \xi,\xi'}} C_i^{(n,\xi,\xi')}X_{i,\alpha}^{\xi}[O_{i,\alpha}^{(n,\xi')}(\mathbf{S})]^* \tag{2}$$

or

$$\mathcal{H}_{\rm SL}=\sum_{\substack{n,i,\alpha\\ \xi,\xi'}} G_i^{(n,\xi,\xi')}\varepsilon_{i,\alpha}^{\xi}[O_{i,\alpha}^{(n,\xi')}(\mathbf{S})]^* \ , \tag{3}$$

where the $C_i^{(n,\xi,\xi')}$ are the nth-order spin-lattice coefficients related to stress, and the $G_i^{(n,\xi,\xi')}$ are those related to strain, corresponding to the ith irreducible representation of the point group of the ion. The $\varepsilon_{i,\alpha}^{\xi}$, $X_{i,\alpha}^{\xi}$, and $O_{i,\alpha}^{(n,\xi')}(\mathbf{S})$ are linear combinations of strain components, stresses, and nth-order spin operators, respectively, transforming as the basis of the ith irreducible representation.

Most of the measurements of spin-lattice coefficients[4-13] have been performed for paramagnetic ions in sites of cubic symmetry, mainly because the number of those coefficients decrease for higher symmetries, and the experiments required for their obtention are simpler. However, studies of ions in lower-symmetry sites, provide wider information about the spin-lattice interaction, and then, they give more chances to test the theory. We published earlier[14] a preliminary study of the spin-lattice interaction of Mn^{2+} in $CaCO_3$, where we reported experiments with the stress applied along the c axis of the crystal. From those experiments, and using complementary published data,[15] we evaluated two of the spin-lattice coefficients. Those results, together with the zero-field splitting parameter D of Mn^{2+} in calcite were used by Yu and Zhao[16] as an effective way to decide the relative importance of the various mechanisms contributing to the zero-field splitting.

We report here a comprehensive study of Mn^{2+} in $CaCO_3$ under uniaxial stress. We applied stress in the three directions (parallel to the c axis, to a cleavage plane, and to a cleavage edge) where calcite accepts high stresses, obtaining six second-order spin-lattice coefficients, and two conditions relating the other four. We use the obtained data to analyze changes in the properties of the Mn^{2+} spectra when displacements of the CO_3^{2-} ions surrounding the Mn^{2+} occur.

II. THE SPIN-LATTICE HAMILTONIAN FOR Mn^{2+} IN $CaCO_3$

The electron-paramagnetic-resonance (EPR) spectrum of Mn^{2+} in $CaCO_3$ has been studied by many authors and it is now well understood.[14,15,17-23]

The crystallographic properties of calcite are well known and were studied elsewhere.[17,18,24] The unit cell is shown in Fig. 1. It contains two inequivalent sites for Ca^{2+}, where Mn^{2+} substitutes Ca^{2+} with equal probability.[19] The point symmetry group for Ca^{2+} (Mn^{2+}) is S_6 (C_{3i}). We choose a set of orthogonal Cartesian coordinates $x_C y_C z_C$ shown in the same figure, as a reference frame for our Hamiltonians and experiments. It is important to note that the y_C axis in our reference frame is along the C_2' symmetry axis.

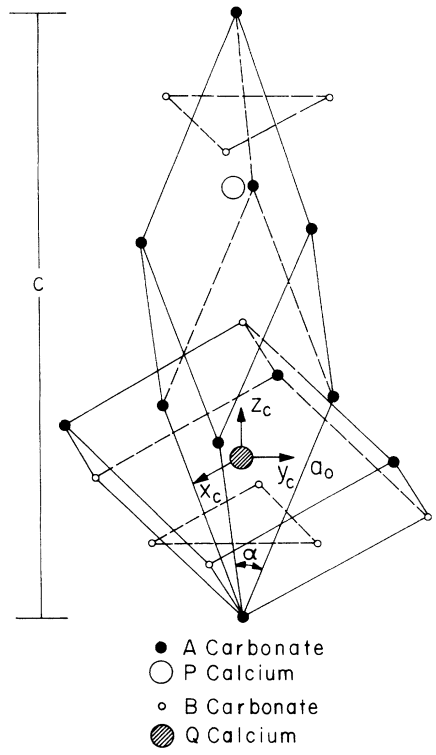

FIG. 1. The unit cell of calcite, together with the cleavage cell. One of the Ca^{2+} sites is shown including the orthogonal system of axes used in this work.

TABLE I. (Top) Normal stresses and strains (Ref. 31) transforming like irreducible representations of the point group S_6. (Bottom) Spin operators transforming like irreducible representations of the point group S_6.

$X_A^{(1)}=X_1+X_2+X_3$	$\varepsilon_A^{(1)}=\varepsilon_1+\varepsilon_2+\varepsilon_3$
$X_A^{(2)}=\frac{1}{2}(2X_3-X_1-X_2)$	$\varepsilon_A^{(2)}=\frac{1}{2}(2\varepsilon_3-\varepsilon_1-\varepsilon_2)$
$X_{C_1}^{(1)}=\sqrt{\frac{3}{8}}(X_1-X_2+i2X_6)$	$\varepsilon_{C_1}^{(1)}=\sqrt{\frac{3}{8}}(\varepsilon_1-\varepsilon_2+i\varepsilon_6)$
$X_{C_1}^{(2)}=\sqrt{\frac{3}{2}}(X_5-iX_4)$	$\varepsilon_{C_1}^{(2)}=\sqrt{\frac{3}{2}}(\varepsilon_5-i\varepsilon_4)$
$X_{C_2}^{(1)}=\sqrt{\frac{3}{8}}(X_1-X_2-i2X_6)$	$\varepsilon_{C_2}^{(1)}=\sqrt{\frac{3}{8}}(\varepsilon_1-\varepsilon_2-i\varepsilon_6)$
$X_{C_2}^{(2)}=\sqrt{\frac{3}{2}}(X_5+iX_4)$	$\varepsilon_{C_2}^{(2)}=\sqrt{\frac{3}{2}}(\varepsilon_5+i\varepsilon_4)$

$$O_A^{(2,1)}(\mathbf{S})=\alpha Y_2^0(\mathbf{S})=\mathcal{O}_2^0(\mathbf{S})$$
$$O_{C_1}^{(2,1)}(\mathbf{S})=\alpha Y_2^2(\mathbf{S})=\frac{1}{\sqrt{2}}[\mathcal{O}_2^2(\mathbf{S})+i\mathcal{S}_2^2(\mathbf{S})]$$
$$O_{C_1}^{(2,2)}(\mathbf{S})=\alpha Y_2^{-1}(\mathbf{S})=\frac{1}{\sqrt{2}}[\mathcal{O}_2^1(\mathbf{S})-i\mathcal{S}_2^1(\mathbf{S})]$$
$$O_{C_2}^{(2,1)}(\mathbf{S})=\alpha Y_2^{-2}(\mathbf{S})=\frac{1}{\sqrt{2}}[\mathcal{O}_2^2(\mathbf{S})-i\mathcal{S}_2^2(\mathbf{S})]$$
$$O_{C_2}^{(2,2)}(\mathbf{S})=\alpha Y_2^1(\mathbf{S})=\frac{1}{\sqrt{2}}[\mathcal{O}_2^1(\mathbf{S})+i\mathcal{S}_2^1(\mathbf{S})]$$
$$\alpha=\sqrt{4\pi/(2l+1)}$$

The complex conjugate irreducible representations C_1 and C_2 imply that

$$X_{C_1}^{(2,\xi,\xi')}=[X_{C_2}^{(2,\xi,\xi')}]^* ,$$
$$O_{C_1}^{(2,\xi,\xi')}=[O_{C_2}^{(2,\xi,\xi')}]^* ,$$

and, since $\mathcal{H}_{SL}$ should be real, we must have

$$C_{C_1}^{(2,\xi,\xi')}=[C_{C_2}^{(2,\xi,\xi')}]^*$$

so we can define the real spin-lattice coefficients $C_{E_1}^{(2,\xi,\xi')}$ and $C_{E_2}^{(2,\xi,\xi')}$ by the equations

$$C_{C_1}^{(2,\xi,\xi')}=C_{E_1}^{(2,\xi,\xi')}-iC_{E_2}^{(2,\xi,\xi')} ,$$
$$C_{C_2}^{(2,\xi,\xi')}=C_{E_1}^{(2,\xi,\xi')}+iC_{E_2}^{(2,\xi,\xi')} .$$

Setting this definition in Eq. (2) and using Table I, where we wrote the linear combinations of components of the stress (strain) tensor, and the second-order spin operators transforming like the irreducible representations of the S_6 point group in the reference frame chosen, we develop the spin-lattice Hamiltonian as

$$\begin{aligned}\mathcal{H}_{SL}=&C_A^{(2,1,1)}\mathcal{O}_2^0(X_1+X_2+X_3)+\tfrac{1}{2}C_A^{(2,2,1)}\mathcal{O}_2^0(2X_3-X_1-X_2)\\&+\sqrt{3}\{C_{E_1}^{(2,1,1)}[\mathcal{O}_2^{2\frac{1}{2}}(X_1-X_2)+\mathcal{S}_2^2X_6]+C_{E_2}^{(2,1,1)}[\mathcal{O}_2^2X_6-\mathcal{S}_2^{2\frac{1}{2}}(X_1-X_2)]\\&+C_{E_1}^{(2,2,1)}[\mathcal{O}_2^2X_5-\mathcal{S}_2^2X_4]+C_{E_2}^{(2,2,1)}[-\mathcal{O}_2^2X_4-\mathcal{S}_2^2X_5]\\&+C_{E_1}^{(2,1,2)}[\mathcal{O}_2^{1\frac{1}{2}}(X_1-X_2)-\mathcal{S}_2^1X_6]+C_{E_2}^{(2,1,2)}[\mathcal{O}_2^1X_6+\mathcal{S}_2^{1\frac{1}{2}}(X_1-X_2)]\\&+C_{E_1}^{(2,2,2)}[\mathcal{O}_2^1X_5+\mathcal{S}_2^1X_4]+C_{E_2}^{(2,2,2)}[-\mathcal{O}_2^1X_4+\mathcal{S}_2^1X_5]\}\\&+\text{fourth-order terms} .\end{aligned} \tag{4}$$

In this work we used the Darwin[25] definition for the spherical harmonics to define the spin operators and their normalization (see Table I).

Equation (4) is the perturbation introduced by stresses on the energy levels of one of the sites occupied by Mn^{2+} in $CaCO_3$; as both sites differ by and operation C_2', the application of such operation on Eq. (4) gives us the perturbation for the other site. This operation is not contained in the point group S_6, and changes the sign of every term in Eq. (4) containing $C_{E_2}^{(2,\xi,\xi')}$. If we assume, as an approximation, that the group is D_{3d}, instead of S_6, all those terms should disappear of Eq. (4). As our Ca sites differ only from D_{3d} by the shapes of the carbonate ions, we could predict that the $C_{E_2}^{(2,\xi,\xi')}$ parameters will be smaller than the others.

As Mn^{2+} has a ${}^6S_{5/2}$ ground state, the main contribution to the energy of its levels in our experiments is the Zeeman interaction. We assumed that eigenstates of S_z, when z is parallel to the magnetic-field direction, are good zeroth-order eigenstates for our perturbation treatment, which takes into account the crystal field and the small changes generated in it by the strain [Eq. (4)]. We calculated the energies to first order in perturbation, and the diagonal part of $\mathcal{H}_{SL}$ in this case is

$$\mathcal{H}_{SL}^{D}=\mathcal{C}_2^0(\mathbf{S})f_2(C_{\Gamma_i}^{(2,\xi,\xi')},X,\theta,\phi)+\mathcal{C}_4^0(\mathbf{S})f_4(C_{\Gamma_i}^{(4,\xi,\xi')},X,\theta,\phi)\ , \tag{5}$$

where θ and ϕ are the polar angles defining the orientation of the magnetic field with respect to our reference frame. Using the rules for rotation of the spherical harmonics (spin operators) we can write

$$\begin{aligned}f_2=&[C_A^{(2,1,1)}(X_1+X_2+X_3)+\tfrac{1}{2}C_A^{(2,2,1)}(2X_3-X_1-X_2)]\tfrac{1}{4}(1+3\cos2\theta)\\&+[C_{E_2}^{(2,1,1)}X_6+\tfrac{1}{2}C_{E_1}^{(2,1,1)}(X_1-X_2)+C_{E_1}^{(2,2,1)}X_5-C_{E_2}^{(2,2,1)}X_4]\tfrac{3}{4}\cos2\phi(1-\cos2\theta)\\&+[-\tfrac{1}{2}C_{E_2}^{(2,1,1)}(X_1-X_2)+C_{E_1}^{(2,1,1)}X_6-C_{E_1}^{(2,2,1)}X_4-C_{E_2}^{(2,2,1)}X_5]\tfrac{3}{4}\sin2\phi(1-\cos2\theta)\\&+[\tfrac{1}{2}C_{E_2}^{(2,1,2)}(X_1-X_2)-C_{E_1}^{(2,1,2)}X_6+C_{E_1}^{(2,2,2)}X_4+C_{E_2}^{(2,2,2)}X_5]\tfrac{3}{2}\sin\phi\sin2\theta\\&+[C_{E_2}^{(2,1,2)}X_6+\tfrac{1}{2}C_{E_1}^{(2,1,2)}(X_1-X_2)+C_{E_1}^{(2,2,2)}X_5-C_{E_2}^{(2,2,2)}X_4]\tfrac{3}{2}\cos\phi\sin2\theta\ .\end{aligned} \tag{6}$$

Since our experimental accuracy does not allow us to evaluate the fourth-order coefficients $C_{\Gamma_i}^{(4,\xi,\xi')}$, it is not useful to give here the expression for f_4.

We now calculate the matrix elements of our spin operators, in order to obtain the effect of Eq. (5) on the Mn^{2+} levels. We obtain

$$\Delta E_{M\leftrightarrow M-1}=\tfrac{3}{2}(2M-1)f_2(C_{\Gamma_i}^{(2,\xi,\xi')},X,\theta,\phi)+\tfrac{1}{8}(140M^3-210M^2-335M+\tfrac{405}{2})\times f_4(C_{\Gamma_i}^{(4,\xi,\xi')},X,\theta,\phi) \tag{7}$$

and the magnetic-field shifts, which are observed in the experiments are

$$\Delta H_{M\leftrightarrow M-1}=-\frac{1}{g\beta}\Delta E_{M\leftrightarrow M-1}\ . \tag{8}$$

Equations (6)–(8) will allow us to obtain the second-order coefficients, as is demonstrated below.

III. EXPERIMENTAL RESULTS

The EPR measurements were performed with an X-band Varian spectrometer and a 12-inch rotating magnet. The uniaxial stress system is similar to that described by Fainstein and Oseroff[26] and allows one to apply stresses along a direction normal to the plane of rotation of the magnetic field. The lineshifts were corrected for the shifts on the resonance frequency of the cavity produced by the stress.

The $CaCO_3$ samples used in our experiments were obtained by cleaving and polishing pieces of a big natural single crystal which showed no defects and contains Mn^{2+} as a natural impurity. When needed, the orientation of the samples was done with Laue photographs: The uncertainty on the orientation of the samples was less than 1°.

The samples support high stresses (up to 10^9 dyn/cm^2) when they are applied along the c-crystal axis, along directions perpendicular to the cleavage faces or along directions parallel to cleavage edges. The line shifts of the five fine-structure lines corresponding to a hyperfine group of the EPR spectrum of Mn^{2+} were measured as a function of stress for stresses applied along each of these three directions, for different orientations of the magnetic field.

Since for most orientations of the magnetic field the EPR lines corresponding to the same transition but different ion sites are partially superposed, it was necessary to separate them by a minimization program which compares the observed line with a linear combination of two Gaussian derivatives, where the separation and width of the two Gaussians were adjustable parameters. The accuracy and reproducibility of the values obtained by this method for the position and linewidth of both resonance lines is very good. This calculation was performed for each magnitude and direction of the applied stress and each orientation of the magnetic field. In some cases the resonances corresponding to both sites overlap at zero stress but are resolved at high stress; in other cases the situation was the opposite.

A linear dependence of line shifts versus stress was observed in all cases within experimental errors. Also, it was observed that the $-\frac{1}{2}\leftrightarrow\frac{1}{2}$ fine-structure transitions are not shifted with stress and the different hyperfine groups of the EPR spectrum are shifted as a whole. These results indicate that the Zeeman and hyperfine terms of the spin-Hamiltonian of Mn^{2+} in $CaCO_3$ are not changed by the stress and the observed line shifts can be explained by Eq. (4), where only fine-structure terms are considered.

In order to interpret the experimental values, Eq. (8) will now be written down for each direction of the applied stress.

A. Stress P along the c-crystal axis

In this simple case, $X_3=-P$, $X_1=X_2=X_4=X_5=X_6=0$, where the negative sign in X_3 indicates a

compressive stress.

The shifts in magnetic field of the fine-structure lines per unit stress, when the field is perpendicular to the applied stress are

$$\frac{\Delta H_{M\leftrightarrow M-1}}{P}=\frac{3}{4g\beta}(2M-1)(C_A^{(2,1,1)}+C_A^{(2,2,1)}) + \frac{1}{8}\left[140M^3-210M^2-335M+\frac{405}{2}\right]\frac{\gamma}{g\beta} . \tag{9}$$

The first term of $\Delta H_{M\leftrightarrow M-1}$ in Eq. (9) is the second-order contribution to the shift; the second one gives the contribution of fourth-order terms of $\mathcal{H}_{SL}$. Both contributions are isotropic in this case. The constant γ stays for a linear combination of fourth-order spin-lattice coefficients.

B. Stress *P* normal to a cleavage plane

The direction of the normal to the cleavage faces of $CaCO_3$ in the crystal coordinate system is given by $\theta=\alpha=63,8°$ and $\phi=0$.[24] Then

$$X_1=-\sin^2\alpha P\ ,\quad X_3=-\cos^2\alpha P\ ,\quad X_5=-\sin\alpha\cos\alpha P\ ; \tag{10}$$
$$X_2=X_4=X_6=0\ .$$

Figure 2(a) shows the direction where the stress is applied and the cleavage plane, where the magnetic field is allowed to rotate. To define the orientation of **H** within this plane only one angle ξ is necessary. As shown in Fig. 2(a), ξ was chosen so that $\xi=0$ is the intersection of the cleavage plane with the crystalline x_cz_c plane. It is easily found that $\sin\xi=\sin\theta\ \sin\phi$ and $\cos\xi=-\cos\theta/\sin\alpha$, where θ and ϕ define the orientation of the applied magnetic field in the $x_Cy_Cz_C$ coordinate system of Fig. 2(a). In terms of the angle ξ, the shifts per unit stress of the fine structure are

$$\frac{\Delta H_{M\leftrightarrow M-1}}{P}=\frac{3(2M-1)}{2g\beta}[A_\xi+B_\xi\cos2\xi\pm C_\xi\sin2\xi] + \frac{1}{8g\beta}\left[140M^3-210M^2-335M+\frac{405}{2}\right] \times(E_\xi+F_\xi\cos2\xi\pm G_\xi\sin2\xi + H_\xi\cos4\xi\pm I_\xi\sin4\xi)\ , \tag{11}$$

where

$$A_\xi=0.1038C_A^{(2,1,1)}-0.0236C_A^{(2,2,1)} -0.2431C_{E_1}^{(2,1,1)}-0.2392C_{E_1}^{(2,2,1)} -0.2392C_{E_1}^{(2,1,2)}-0.2354C_{E_1}^{(2,2,2)}\ , \tag{11a}$$

$$B_\xi=0.6038C_A^{(2,1,1)}-0.1253C_A^{(2,2,1)} +0.3608C_{E_1}^{(2,1,1)}+0.3550C_{E_1}^{(2,2,1)} -0.2392C_{E_1}^{(2,1,2)}-0.2354C_{E_1}^{(2,2,2)}\ , \tag{11b}$$

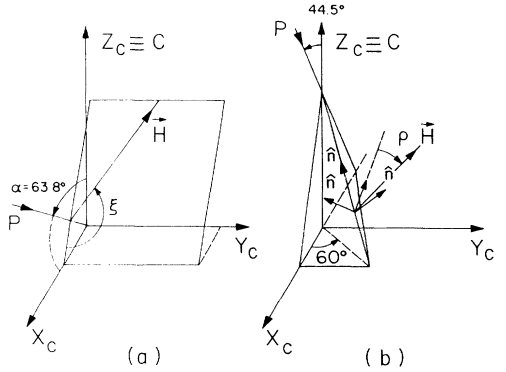

FIG. 2. Relative orientation of the magnetic field with respect to the crystal axes: (a) when the experiment is performed in the cleavage plane; (b) when it is performed in a plane perpendicular to the cleavage edge.

$$C_\xi=-0.2666C_{E_2}^{(2,1,1,)}-0.2623C_{E_2}^{(2,2,1)} -0.5418C_{E_2}^{(2,1,2)}-0.5331C_{E_2}^{(2,2,2)}\ . \tag{11c}$$

The coefficients E_ξ, F_ξ, G_ξ, H_ξ, and I_ξ in Eq. (11) are linear combinations of fourth-order spin-lattice coefficients. The double sign ($\pm$) in C_ξ, G_ξ, and I_ξ fixes the difference between the two inequivalent sites. In our Figs. 3–6, site 1 refers to the plus sign and site 2 to the minus sign.

C. Stress *P* parallel to a cleavage edge

The direction $\hat{n}$ of a cleavage edge, defined by the intersection of two cleavage faces is given by [see Fig. 2(b)]

$$\hat{n}=\frac{\hat{n}_1\times\hat{n}_2}{|\hat{n}_1\times\hat{n}_2|}\ ,$$

where $\hat{n}_1=(\sin\alpha,\ 0,\ \cos\alpha)$ and $\hat{n}_2$

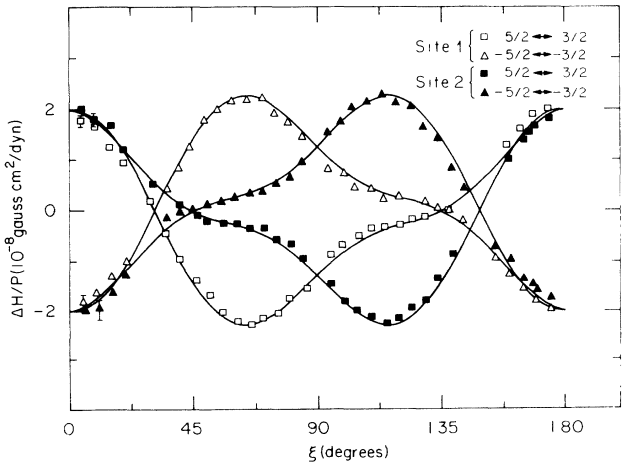

FIG. 3. Angular variation of the line shifts under stress when pressure is applied perpendicular to the cleavage plane of calcite; the effect on the $Mn^{2+}|\pm5/2,\pm5/2\rangle\leftrightarrow|\pm3/2,\pm5/2\rangle$ transitions are shown.

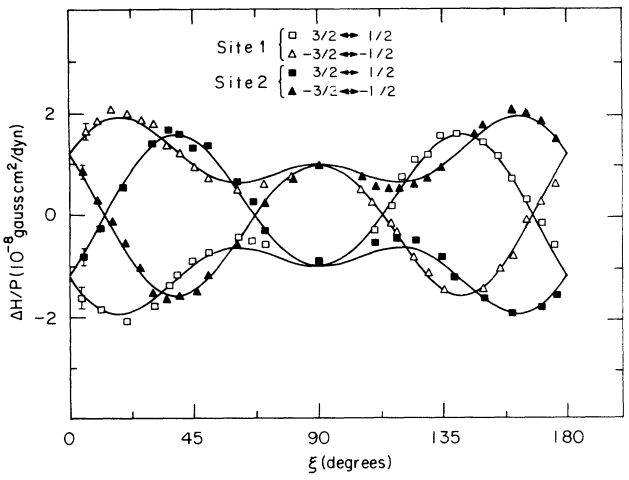

FIG. 4. Same as Fig. 3, showing the $|\pm 3/2, \pm 5/2\rangle \leftrightarrow |\pm 1/2, \pm 5/2\rangle$ Mn^{2+} transitions.

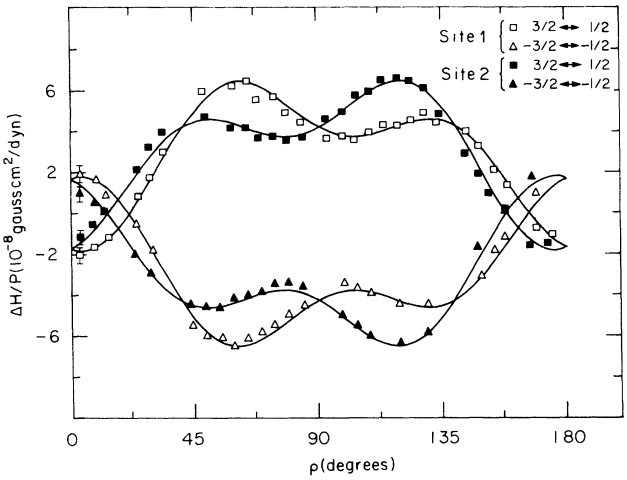

FIG. 6. Same as Fig. 4, when the stress is applied parallel to a cleavage edge.

$=[-\frac{1}{2}\sin\alpha, (\sqrt{3}/2)\sin\alpha, \cos\alpha]$ are the normal to the cleavage faces and $\alpha = 63, 8°$.

One finds $\theta_0 = 44.5°$ and $\phi_0 = 240°$ for the direction of $\hat{n}$ and then the values of the components of the stress tensor are

$$X_1 = -\sin^2\theta_0\cos^2\phi_0 P \ , \quad X_6 = -\sin^2\theta_0\sin\phi_0\cos\phi_0 P \ ,$$
$$X_2 = -\sin^2\theta_0\sin^2\phi_0 P \ , \quad X_5 = -\sin\theta_0\cos\theta_0\cos\phi_0 P \ , \qquad (12)$$
$$X_3 = -\cos^2\theta_0 P \ , \quad X_4 = -\sin\theta_0\cos\theta_0\sin\phi_0 P \ .$$

The plane of rotation of the magnetic field is in this case perpendicular to the cleavage edge and the direction of **H** may be specified by an angle ρ on this plane. As shown in Fig. 2(b) we choose ρ in such a way that $\rho = 0$ is the direction of the intersection of the plane normal to the cleavage edge with the plane determined by the cleavage edge and the c-crystal axis (z_c).

If the orientation of the magnetic field is given by the angles θ and ϕ, it can be proved that

$$\sin\theta\cos\phi = -\cos\theta_0\cos\phi_0\cos\rho + \sin\phi_0\sin\rho \ ,$$
$$\sin\theta\sin\phi = -\cos\theta_0\sin\phi_0\cos\rho - \cos\phi_0\sin\rho \ , \qquad (13)$$
$$\cos\theta = \sin\theta_0\cos\rho \ .$$

Equations (12) and (13) are used to write the spin-lattice Hamiltonian of Eq. (4) as a function of ρ when the external stress is applied along a cleavage edge.

The shifts per unit stress of the fine-structure transitions obtained from Eq. (8) for this particular geometry are, as a function of ρ,

$$\frac{\Delta H_{M\leftrightarrow M-1}}{P} = \frac{3}{2g\beta}(2M-1)[A_\rho + B_\rho\cos 2\rho \pm C_\rho\sin 2\rho] + \frac{1}{8g\beta}\left[140M^3 - 210M^2 - 335M + \frac{405}{2}\right] \times [E_\rho + F_\rho\cos 2\rho \pm G_\rho\sin 2\rho + H_\rho\cos 4\rho \pm I_\rho\sin 4\rho] \ , \qquad (14)$$

where

$$A_\rho = -0.1315C_A^{(2,1,1)} - 0.0346C_A^{(2,2,1)} - 0.0905C_{E_1}^{(2,1,1)} - 0.1842C_{E_1}^{(2,2,1)} - 0.1842C_{E_1}^{(2,1,2)} - 0.3749C_{E_1}^{(2,2,2)} \ , \qquad (14a)$$

$$B_\rho = 0.3685C_A^{(2,1,1)} + 0.0970C_A^{(2,2,1)} + 0.2780C_{E_1}^{(2,1,1)} + 0.5657C_{E_1}^{(2,2,1)} - 0.1842C_{E_1}^{(2,1,2)} - 0.3749C_{E_1}^{(2,2,2)} \ , \qquad (14b)$$

$$C_\rho = -0.2628C_{E_2}^{(2,1,1)} - 0.5349C_{E_2}^{(2,2,1)} - 0.2583C_{E_2}^{(2,1,2)} - 0.5256C_{E_2}^{(2,2,2)} \ , \qquad (14c)$$

where the same remarks made about the double sign ($\pm$) in Eq. (11) apply here.

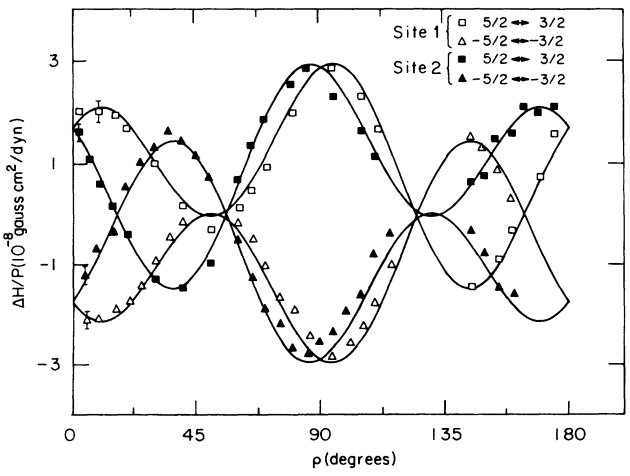

FIG. 5. Same as Fig. 3, when the stress is applied parallel to a cleavage edge.

D. Results of the experiments

Our results for the shift per unit stress of the four fine-structure lines of Mn^{2+} in $CaCO_3$ corresponding to the two different sites are shown in Figs. 3 and 4 as a function of ξ, for stress applied perpendicular to the cleavage plane, and in Figs. 5 and 6 as a function of ρ for stress applied along the cleavage edge. Care has been taken on labeling different sites for Mn^{2+} in order to use the correct sign in Eqs. (11) and (14) for each site.

A least-squares fitting with Eq. (11) was performed to the data plotted in Figs. 3 and 4, where the calculated curves are also displayed. From this fitting we obtained the following values for the second- and fourth-order contributions:

$$\begin{aligned}
A_\xi &= -(0.057\pm0.003)\times10^{-12}\ \text{cm/dyn}\ , \\
B_\xi &= (0.174\pm0.005)\times10^{-12}\ \text{cm/dyn}\ , \\
C_\xi &= -(0.188\pm0.010)\times10^{-12}\ \text{cm/dyn}\ , \\
E_\xi &= (0.006\pm0.005)\times10^{-12}\ \text{cm/dyn}\ , \\
F_\xi &= (0.016\pm0.005)\times10^{-12}\ \text{cm/dyn}\ , \\
G_\xi &= (0.015\pm0.003)\times10^{-12}\ \text{cm/dyn}\ , \\
H_\xi &= (0.017\pm0.003)\times10^{-12}\ \text{cm/dyn}\ , \\
I_\xi &= (0.013\pm0.010)\times10^{-12}\ \text{cm/dyn}\ .
\end{aligned} \tag{15}$$

F_ξ, G_ξ, and H_ξ give contributions which are well out of the experimental errors, indicating that fourth-order contributions in $\mathcal{H}_{SL}$ are important. However, E_ξ and I_ξ are completely inside experimental error.

A least-squares fitting of the experimental data of Figs. 5 and 6 with Eq. (14) gives the following values for the second- and fourth-order contributions:

$$\begin{aligned}
A_\rho &= (0.37\pm0.05)\times10^{-12}\ \text{cm/dyn}\ , \\
B_\rho &= (-0.33\pm0.03)\times10^{-12}\ \text{cm/dyn}\ , \\
C_\rho &= (0.092\pm0.008)\times10^{-12}\ \text{cm/dyn}\ , \\
E_\rho &= (-0.047\pm0.007)\times10^{-12}\ \text{cm/dyn}\ , \\
F_\rho &= (0.048\pm0.003)\times10^{-12}\ \text{cm/dyn}\ , \\
G_\rho &= (0.001\pm0.0030)\times10^{-12}\ \text{cm/dyn}\ , \\
H_\rho &= (0.045\pm0.040)\times10^{-12}\ \text{cm/dyn}\ , \\
I_\rho &= (0.023\pm0.005)\times10^{-12}\ \text{cm/dyn}\ ,
\end{aligned} \tag{16}$$

and also gives nonnegligible fourth-order contributions. We show in Figs. 5 and 6 the curves obtained with the fitting.

Our measurements of the shifts of the fine-structure lines of Mn^{2+} in $CaCO_3$ with stresses applied along the c axis were reported previously;[14] the shifts are isotropic when the magnetic field is in the plane perpendicular to the stress [as given in Eq. (9)] and allow us to obtain

$$C_A^{(2,1,1)}+C_A^{(2,2,1)}=(-1.43\pm0.06)\times10^{-13}\ \text{cm/dyn} \tag{17}$$

and the value of γ in Eq. (9) is inside of experimental uncertainty.

Our experimental results of Eq. (15)–(17) may be substituted in Eqs. (11a), (11b), (14a), and (14b) together with the results of the hydrostatic stress-EPR experiments reported by Wait.[15] In that way we obtained the values of the two $C_A^{(2,\xi,\xi')}$ and the four $C_{E_1}^{(2,\xi,\xi')}$ spin-lattice coefficients, which are tabulated in Table II. In addition, we obtained the values of two linear combinations of the other four $C_{E_2}^{(2,\xi,\xi')}$ coefficients, which are also given in Table II.

It is worth noting that we found it impossible to perform experiments with the stress in other directions than those reported here. In every case the samples became brittle and they broke in small pieces for stresses of the order of 5×10^6 dyn/cm^2, even when the stress is applied only a few degrees apart from the directions described before.

IV. DISCUSSION

An evaluation of the spin-Hamiltonian or the spin-lattice Hamiltonian parameters for S-state ions should include high-order perturbation calculations involving the crystalline electric field, the spin-orbit, and the spin-spin interactions, and also other relativistic mechanisms. Good examples were given by Wybourne[27] for Gd^{3+}, by Sharma, Das, and Orbach[28] for Mn^{2+} ions, and, more recently, by Yu and Zhao for Mn^{2+} ions in calcite.[16] These calculations are very complicated and the results are, in general, not very rewarding: In many cases the results differ from the experimental values in the order of magnitude and even in the sign. We believe, however, that a phenomenological analysis of the data is very helpful to understand the problem and the conclusions may be extended to other low-symmetry crystals.

It is important to remark first that our experiments show a linear dependence of the line shifts with stress.

TABLE II. Second-order spin-lattice coefficients.

$(\text{cm/dyn})\times10^{-12}$	
$C_A^{(2,1,1)}=-0.0011\pm0.0001$	$C_A^{(2,2,1)}=-0.142\pm0.007$
$C_{E_1}^{(2,1,1)}=2.42\pm0.23$	$C_{E_1}^{(2,2,1)}=-2.09\pm0.22$
$C_{E_1}^{(2,1,2)}=0.78\pm0.26$	$C_{E_1}^{(2,2,2)}=-0.91\pm0.25$
$0.266\ C_{E_2}^{(2,1,1)}+0.262C_{E_2}^{(2,2,1)}+0.542C_{E_2}^{(2,1,2)}+0.533C_{E_2}^{(2,2,2)}=0.188\pm0.008$	
$0.263\ C_{E_2}^{(2,1,1)}+0.535C_{E_2}^{(2,2,1)}+0.258C_{E_2}^{(2,1,2)}+0.526C_{E_2}^{(2,2,2)}=-0.092\pm0.010$	

Since Zaitov[29] reported a nonlinear stress dependence for Mn^{2+} in calcite crystals, we studied carefully this behavior, without finding any nonlinear dependence. This observation, which was reported previously by us for the stress parallel to the c-crystal axis,[14] was verified along this work for stresses applied in other crystal directions. It indicates a small magnitude for the covalent effects in the bonding between Mn^{2+} and its CO_3^{2-} neighbors.

A. The A-mode spin-lattice coefficients

The $C_A^{(2,\xi,\xi')}$ and $G_A^{(2,\xi,\xi')}$ were previously analyzed[14] and in Table II we repeat the values of the $C_A^{(2,\xi,\xi')}$ (the difference from Ref. 14 stems from the normalization we use here for $\mathcal{C}_2^0$). The values of $G_A^{(2,\xi,\xi')}$ are

$$G_A^{(2,2,1)} \cong -8\times 10^{-2}\ \text{cm}^{-1}\ ,$$

$$G_A^{(2,1,1)} \cong 3\times 10^{-2}\ \text{cm}^{-1}\ .$$

We do not give the errors of the $G_A^{(2,\xi,\xi')}$ because the relative errors are high; this is due to the accumulation of errors in going from the C_{ij},[30] through S_{ij}, to the $G_A^{(2,\xi,\xi')}$.

It is worth mentioning at this point the work of Yu and Zhao,[16] where our previous results[14] of the A-mode spin-lattice coefficients are theoretically analyzed. They consider several mechanisms in order to calculate those parameters, following their own theoretical model, which is slightly different from previous calculations. Considering the spin-orbit coupling as the most important of the contributions, they obtain good agreement with the experiments.

B. The E-mode second-order spin-lattice coefficients

We present the results of two hypothetical experiments that will allow us to evaluate the importance of the carbonate distortions to the EPR spectrum.

Initially we show that our results are consistent. Let us assume that the effect of the local distortions of one carbonate modify much less the EPR spectra than changes in the position of the whole carbonate; this is equivalent to assume that the local symmetry is D_{3d}. Let us apply a hypothetical stress to our system. Making $X_1=P$, $X_2=-P$ and all the other stresses null, substituting those in the spin-lattice Hamiltonian, and orienting the magnetic field in the direction of maximum line shift ($\theta=\pi/2$, $\phi=0$), we get

$$\Delta H/P = -\frac{(2M-1)}{g\beta}[0.50\pm 0.21]$$

$$\times 10^{-11}\ \text{Gauss cm}^2/\text{dyn}$$

expression to be compared with the observed effect [derived from Eq. (17)] when the stress is applied parallel to the c axis:

$$\Delta H/P = -\frac{(2M-1)}{g\beta}[0.107\pm 0.004]$$

$$\times 10^{-12}\ \text{Gauss cm}^2/\text{dyn}\ .$$

We can easily see that the shifts resulting from the E-mode distortions are one order of magnitude greater than those of A-mode. This corresponds clearly with the fact that the crystal as a whole is "soft" in front to stresses applied in any other directions than those applied in our experiments. This result shows the consistency of our results.

Now we can evaluate, by another ideal experiment, the importance of the distortion of the carbonate ions relative to their rigid displacement. Fortunately it is possible to obtain from the two equations relating the $C_{E_2}^{(2,\xi,\xi')}$ parameters a useful linear combination of only two of them:

$$C_{E_2}^{(2,1,2)} - C_{E_2}^{(2,2,1)} = (1.004\pm 0.065)\times 10^{-12}\ \text{cm/dyn}\ .$$

Now we can make a calculation that assumes full S_6 symmetry if we choose a system of stresses and a direction for the magnetic field so that only this specific linear combination of $C_{E_2}^{(2,\xi,\xi')}$ parameters appears in $\mathcal{H}_{\text{SL}}$. It is not difficult to see that assuming $X_1=(2/3)P$, $X_2=-(2/3)P$, $X_4=-(4/3)P$ and all the other stresses zero, with the field in the direction $\theta=\pi/4$ and $\phi=\pi/2$, we eliminate all the unknowns and obtain

$$\Delta H/P = -\frac{(2M-1)}{g\beta}[2.40\pm 0.68]$$

$$\times 10^{-12}\ \text{Gauss cm}^2/\text{dyn}\ .$$

We can now assume D_{3d} symmetry (all $C_{E_2}^{(2,\xi,\xi')}=0$) and calculate the shifts for the same system of stresses and position of magnetic field. We obtain

$$\Delta H/P = -\frac{(2M-1)}{g\beta}[0.92\pm 0.62]$$

$$\times 10^{-12}\ \text{Gauss cm}^2/\text{dyn}\ .$$

In spite of the large relative error of the last calculated quantity, by comparison of the two results, there is obviously a large influence of the distortion of the carbonates in front of their rigid displacement.

As a conclusion to this work, we find it important to remark the following.

(a) We studied completely a low-symmetry crystal under stresses. This system taught us many properties of the EPR spectra under stress. Especially, the distortion of the carbonates is very important, as it was seen in the last paragraph above. Different than the observed effect on the unstressed crystal,[19] the nondiagonal parameters obtained are of the same order of magnitude as those related to the higher symmetry.

(b) Many low-symmetry crystals became important because of the physics contained in them. Namely, high-T_c superconductors contain magnetic ions in very low-symmetry sites. We believe that our procedure can be applied to those crystals, doped with magnetic ions. In such a way, different sites could be identified, and the re-

sults used to decide about population of nonequivalent sites.

(c) Our work completes the EPR study of Mn^{2+} in calcite. Six new parameters were reported, complementary to the spin-Hamiltonian coefficients published before.

Finally, we found that local elastic constants are extremely relevant in the microscopic understanding of sites of lower symmetry than that of the whole crystal. X-ray measurements of those constants is relevant to understand the physics of those crystals.

ACKNOWLEDGMENTS

This work was partially supported by Fundação de Amparo à Pesquisa do Estado de São Paulo and Conselho Nacional de Pesquisa e Desenvolvimento (Brazil).

[1]J. F. Nye, *Physical Properties of Crystals* (Oxford, Oxford University Press, 1955).
[2]J. H. Van Vleck, Phys. Rev. **57**, 426 (1940).
[3]R. Orbach and H. J. Stapleton, in *Electron Paramagnetic Resonance*, edited by S. Geschwind (Plenum, New York, 1972).
[4]E. R. Feher, Phys. Rev. **136**, A145 (1964).
[5]R. Calvo, R. A. Isaacson, and Z. Sroubek, Phys. Rev. **177**, 484, (1969).
[6]R. B. Hemphill, P. L. Donoho, and E. D. McDonald, Phys. Rev. **146**, 329 (1966).
[7]G. Watkins and E. Feher, Bull. Am. Phys. Soc. **7**, 29 (1962).
[8]R. Calvo, Z. Sroubek, S. Rubins, and P. Zimmermann, Phys. Lett. **27A**, 143 (1968).
[9]S. Oseroff and R. Calvo, Phys. Rev. B **5**, 2474 (1972).
[10]S. Oseroff and R. Calvo, J. Phys. Chem. Solids **33**, 2275 (1972).
[11]Z. Sroubek, M. Tachiki, P. H. Zimmermann, and R. Orbach, Phys. Rev. **165**, 435 (1968).
[12]R. Calvo, S. Oseroff, M. C. Passeggi, C. Fainstein, and M. Tovar, Phys. Rev. B **9**, 4888 (1974).
[13]J. M. Baker and D. van Ormondt, J. Phys. C **7**, 2060 (1974).
[14]G. E. Barberis and R. Calvo, Solid State Commun. **15**, 173 (1974).
[15]D. F. Wait, Phys. Rev. **132**, 601 (1963)
[16]Yu Wan-Lu and Zhao Min-Guang, J. Phys. C **20**, 4647 (1987).
[17]C. Kikuchi, Phys. Rev. **100**, 1243 (1955); H. M. McConnell, J. Chem. Phys. **24**, 904 (1956).
[18]C. Kikuchi and L. M. Matarresse, J. Chem. Phys. **33**, 601 (1960).
[19]G. E. Barberis, R. Calvo, H. G. Maldonado, and C. Zarate, Phys. Rev. B **12**, 853 (1975).
[20]F. K. Hurd, M. Sachs, and W. D. Hershberger, Phys. Rev. **93**, 373 (1954).
[21]J. A. Hodges, S. A. Marshall, J. A. McMillan, and R. A. Serway, J. Chem. Phys. **49**, 2857 (1968).
[22]L. M. Matarresse, J. Chem. Phys. **34**, 336 (1961).
[23]R. A. Serway, Phys. Rev. B **3**, 608 (1971).
[24]R. W. Wyckoff, *Crystal Structures* (Interscience, New York, 1963).
[25]E. Butkov, *Mathematical Physics* (Addison-Wesley, Reading, MA, 1968), p. 168.
[26]C. Fainstein and S. Oseroff, Rev. Sci. Instrum. **42**, 547 (1971).
[27]B. G. Wybourne, Phys. Rev. **148**, 317 (1966).
[28]R. R. Sharma, T. P. Das, and R. Orbach, Phys. Rev. **149**, 257 (1966); **155**, B38 (1967); see also D. J. Newman, Chem. Phys. Lett. **6**, 288 (1970).
[29]M. M. Zaitov, Fiz. Tverd. Tela. (Leningrad) **9**, 453 (1967) [Sov. Phys. Solid State **9**, 346 (1967)].
[30]D. P. Dandekar, Phys. Rev. **172**, 873 (1968).
[31]To understand the missing factor 2 in $\varepsilon_{C_1}^{(1)}$ and in $\varepsilon_{C_2}^{(1)}$ see Ref. 1, p. 135.